

# Large eddy simulation of stably stratified turbulent open channel flows with low- to high-Prandtl number

Lei Wang, Xi-Yun Lu \*

*Department of Modern Mechanics, University of Science and Technology of China, Hefei, Anhui 230026, China*

Received 12 August 2004; received in revised form 31 December 2004

Available online 25 February 2005

## Abstract

Large eddy simulation of thermally stratified turbulent open channel flows with low- to high-Prandtl number is performed. The three-dimensional filtered Navier–Stokes and energy equations under the Boussinesq approximation are numerically solved using a fractional-step method. Dynamic subgrid-scale (SGS) models for the turbulent SGS stress and heat flux are employed to close the governing equations. The objective of this study is to reveal the effects of both the Prandtl number ( $Pr$ ) and Richardson ( $Ri_\tau$ ) number on the characteristics of turbulent flow, heat transfer, and large-scale motions in weakly stratified turbulence. The stably stratified turbulent open channel flows are calculated for  $Pr$  from 0.1 up to 100,  $Ri_\tau$  from 0 to 20, and the Reynolds number ( $Re_\tau$ ) 180 based on the wall friction velocity and the channel height. To elucidate the turbulent flow and heat transfer behaviors, some typical quantities, including the mean velocity, temperature and their fluctuations, turbulent heat fluxes, and the structures of the velocity and temperature fluctuations, are analyzed.

© 2005 Elsevier Ltd. All rights reserved.

**Keywords:** Large eddy simulation (LES); Thermally stratified turbulence; Stably stratified turbulence; Heat transfer; Turbulent open channel flow; Subgrid scale (SGS) model

## 1. Introduction

Understanding and prediction of turbulent heat and mass transfer processes from a solid boundary and near an interfacial surface are of great interest in both applications and fundamentals. In the problem of heat transfer by fluid flow, the Prandtl number ( $Pr$ ) can range from order of unity or less to hundreds. In the case of the heat transfer at low or moderate Prandtl number, a significant temperature gradient exists not only in the

diffusive sublayer but also in the region outside the sublayer. High-Prandtl number heat transfer is of special importance in the understanding of the heat transfer near a free surface and/or in a turbulent boundary layer flow. The heat diffusive sublayer for the high-Prandtl number heat transfer by the interface or the solid boundary is very thin, and the heat transfer efficiency is primarily controlled by turbulent motions very close to the interface or the boundary. Thus, it is a challenging task to study the heat transfer at high Prandtl number, in particular, considering thermal stratification effect where an active scalar (e.g., thermal energy) is transferred in turbulent boundary layer and/or across the interface.

\* Corresponding author. Tel.: +86 551 3603223; fax: +86 551 3606459.

E-mail address: [xlu@ustc.edu.cn](mailto:xlu@ustc.edu.cn) (X.-Y. Lu).

### Nomenclature

$B$	additive constant in the logarithmic law of the velocity profile	$T_\tau$	friction temperature
$B_T$	additive constant in the logarithmic law of the temperature profile	$u$	resolved streamwise velocity component
$C$	SGS model coefficient	$u_b$	bulk mean velocity
$g$	gravitational acceleration	$\bar{u}_i$	resolved velocity components
$k$	thermal conductivity	$u'_i$	resolved velocity fluctuations
$K$	von Kármán constant in the logarithmic law of the velocity profile	$u_\tau$	friction velocity
$K_T$	von Kármán constant in the logarithmic law of the temperature profile	$v$	resolved spanwise velocity component
$Nu$	Nusselt number	$w$	resolved vertical velocity component
$\bar{p}$	resolved modified pressure	$x$	streamwise coordinate
$Pr$	Prandtl number	$x_i$	Cartesian coordinate axes
$Pr_T$	turbulent Prandtl number	$y$	spanwise coordinate
$q_F$	averaged heat flux through the free surface	$z$	vertical coordinate
$q_i$	SGS turbulent heat flux	$z_B^+$	vertical coordinate normalized by the friction velocity from the wall
$Re_m$	Reynolds number based on the bulk mean velocity	$z_F^+$	vertical coordinate normalized by the friction velocity from the free surface
$Re_\tau$	Reynolds number based on the friction velocity	$\beta$	thermal expansion coefficient
$Ri_g$	local gradient Richardson number	$\delta$	height of the channel
$Ri_\tau$	Richardson number based on the friction velocity	$\delta_{i1}$	delta function along the streamwise direction
$R_{kk}$	trace of SGS Reynolds stress	$\bar{\Delta}$	size of grid filter
$\bar{S}_{ij}$	resolved strain rate tensor	$\hat{\Delta}$	size of test filter
$t$	time	$\tau_{ij}$	SGS turbulent stress tensor
$\bar{T}$	resolved temperature	$\nu$	molecular kinematic viscosity
$T^+$	resolved temperature normalized by the friction temperature	$\kappa$	thermal diffusivity
$T'^+$	resolved temperature fluctuation normalized by the friction temperature	$\langle \rangle$	average in time and in the plane parallel to the wall
$T_B$	temperature at the bottom wall	$\langle \rangle_s$	average in the plane parallel to the wall
$T_F$	temperature at the free surface	<i>Subscript</i>	
		rms	root mean square
		<i>Superscript</i>	
		+	normalized quantity by wall parameters

Thermally stratified turbulent open channel flow is employed as a typical problem to be investigated in this study. Some experiments have been undertaken to reveal the most characteristics of open turbulent flows [1–6]. However, considerable difficulty in making accurate velocity and scalar measurements very near the boundary and the interfacial surface, in particular for high Prandtl number with very thin diffusive sublayer, is unavoidable. To some extent, direct numerical simulation (DNS) approach can be used to analyze the behaviors of turbulence structure and scalar transport near the free surface, allowing precise determination of the velocity field very close to the interfacial surface. Due to the expensive cost of the DNS, some previous work was only limited their investigations to low Reynolds (usually  $Re_\tau \leq 180$ , based on the wall friction velocity and

the channel depth) and Prandtl ( $Pr \leq 2$ ) number. The DNS calculations [8–10] have been performed to deal with turbulence structures near the free surface in an open channel flow with a zero-shear interface. Recently, some work [11,12] has been carried out to study turbulence structure and scalar transport near the free surface in open turbulent channel flows.

In fact, it is obviously impossible to use DNS approach to solve problems in which both the Reynolds and Prandtl numbers are large, since the number of mesh points required to describe all the scales is of order  $Pr^3 Re^{9/4}$ . However, it is now well established that large eddy simulation (LES) technique, which is much cheaper than the DNS since it solves only the large-scale components of turbulent flow and models the subgrid-scale (SGS) effects via SGS models, provides an effective tool

to study some detailed features of turbulent flows. The SGS model is a key problem in the LES. A dynamic SGS model was proposed by Germano et al. [13] which overcome some shortcomings of the classical Smagorinsky model [14]. The dynamic model gained a remarkable success in the past decade and gave a new impetus to the development of reasonable strategies for the LES [15,16]. On account of the improvements made by the SGS models, it becomes highly tempting to use the dynamic SGS model for studying turbulent heat transfer at high Prandtl (or Schmidt) number [17–19]. Furthermore, to obtain reliable LES results for turbulent flow at a free surface, it is needed to ensure that replacing DNS by LES will not produce significant deviation in the large scales of turbulent flow field. Based on recent work [20,21], it is confirmed that, since turbulence distortion is less severe near a free surface than near a solid wall, there is no doubt that the LES approach provides an accurate description of the large-scale dynamics in the surface-influenced region.

Turbulence structure is considerably affected when an active scalar is transferred in turbulent boundary layer and/or across the free surface. Usually, turbulence statistics in stably stratified flows depends on the local Richardson number, defined by the local velocity and temperature gradients, and the effect of thermal stratification plays an important role in the turbulent heat transfer [22–24]. Only have Nagaosa and Saito [25] investigated stably stratified open turbulent channel flow using the DNS for  $Pr = 1$  and  $Ri_\tau = 0, 10$  and  $20$ . They indicated that the turbulence structure and scalar transfer near the free surface in stratified flows are complicated since the stratification influences the turbulence structure, in particular in the turbulent boundary layer near the wall. To the best of our knowledge, however, little work for thermally stratified open turbulent channel flows with low- to high-Prandtl number has been carried out to deal with the characteristics of turbulence and heat transfer. In this study, based on the LES technique, stably stratified turbulent open channel flows for  $Pr$  from 0.1 up to 100,  $Ri_\tau$  from 0 to 20 and  $Re_\tau = 180$  are investigated.

This paper is organized as follows. The mathematical formulation and the dynamic SGS models for modeling SGS turbulent stresses and heat fluxes are described in Section 2. The numerical method is given in Section 3. In Section 4, some typical statistical turbulence and heat transfer quantities are discussed. Finally, concluding remarks are summarized in Section 5.

## 2. Mathematical formulations

To study thermally stratified turbulent open channel flow, the three-dimensional filtered incompressible Navier–Stokes and energy equations under the Boussinesq

approximation are solved. To non-dimensionalize the governing equations, the wall friction velocity  $u_\tau$  is used as the velocity scale, the channel height  $\delta$  as the length scale, and the temperature difference  $\Delta T$  between the free surface ( $T_F$ ) and the bottom wall ( $T_B$ ) as the temperature scale. The non-dimensional governing equations are given as

$$\frac{\partial \bar{u}_i}{\partial x_i} = 0 \quad (1)$$

$$\begin{aligned} \frac{\partial \bar{u}_i}{\partial t} + \frac{\partial}{\partial x_j} (\bar{u}_i \bar{u}_j) \\ = -\frac{\partial \bar{p}}{\partial x_i} + \frac{1}{Re_\tau} \frac{\partial^2 \bar{u}_i}{\partial x_j \partial x_j} - \frac{\partial \tau_{ij}}{\partial x_j} + \delta_{i1} + Ri_\tau \bar{T} \delta_{i3} \end{aligned} \quad (2)$$

$$\frac{\partial \bar{T}}{\partial t} + \frac{\partial (\bar{T} \bar{u}_j)}{\partial x_j} = \frac{1}{Re_\tau Pr} \frac{\partial^2 \bar{T}}{\partial x_j \partial x_j} - \frac{\partial q_j}{\partial x_j} \quad (3)$$

where  $\tau_{ij} = R_{ij} - \delta_{ij} R_{kk}/3$ ,  $R_{ij} = \bar{u}_i \bar{u}_j - \bar{u}_i \bar{u}_j$ ,  $q_j = \bar{T} \bar{u}_j - \bar{T} \bar{u}_j$ , overbar “ $\bar{\cdot}$ ” represents the resolved variable.  $\bar{T} = \bar{T} - \langle \bar{T} \rangle_S$ , and  $\langle \cdot \rangle_S$  stands for an average over a plane parallel to the horizontal wall.  $\bar{u}_i$  and  $\bar{T}$  are the resolved velocity and temperature.  $\bar{p}$  is the resolved modified pressure, which contains a term  $R_{kk}/3$ . In this study, the resolved velocity  $\bar{u}_i$  ( $i = 1, 2, 3$ ), for writing convenience, is represented as  $u$ ,  $v$  and  $w$  in the streamwise ( $x$ ), spanwise ( $y$ ) and vertical ( $z$ ) directions, respectively.  $Re_\tau = u_\tau \delta / \nu$  represents the Reynolds number and  $Pr = \nu / \kappa$  is the molecular Prandtl number with  $\nu$  being the kinematic viscosity and  $\kappa$  the thermal diffusivity.  $Ri_\tau$  is the Richardson number defined as  $Ri_\tau = \beta g \Delta T \delta / u_\tau^2$ , where  $g$  is the gravitational acceleration,  $\beta$  is the thermal expansion coefficient which is assumed to be small enough so that the Boussinesq approximation is applicable.

In Eqs. (2) and (3),  $\tau_{ij}$  and  $q_j$  represent SGS turbulent stress and heat flux, which need to be modeled by SGS models. The overall expressions of the SGS stress and the SGS turbulent heat flux are written as, respectively

$$\tau_{ij} = -2C \bar{\Delta}^2 |\bar{S}| \bar{S}_{ij}, \quad q_j = -\frac{C \bar{\Delta}^2}{Pr_T} |\bar{S}| \frac{\partial \bar{T}}{\partial x_j} \quad (4)$$

where  $\bar{S}_{ij} = \frac{1}{2} \left( \frac{\partial \bar{u}_i}{\partial x_j} + \frac{\partial \bar{u}_j}{\partial x_i} \right)$ ,  $|\bar{S}| = [2\bar{S}_{ij} \bar{S}_{ij}]^{\frac{1}{2}}$ .  $\bar{\Delta}$  is the filter width, and  $Pr_T$  represents the turbulent Prandtl number.

Here, the model coefficients of  $C$  and  $Pr_T$  in Eq. (4) are obtained by use of the approach proposed by Germano et al. [13]. After introducing a test filtering with a filter width  $\hat{\Delta}$  to Eqs. (1)–(3), the coefficients  $C$  and  $Pr_T$  can be dynamically determined as

$$C = -\frac{1}{\hat{\Delta}^2} \frac{\langle L_{ij} M_{ij} \rangle_S}{\langle M_{ij} M_{ij} \rangle_S}, \quad Pr_T = -C \bar{\Delta}^2 \frac{\langle F_i F_i \rangle_S}{\langle E_i F_i \rangle_S} \quad (5)$$

where

$$M_{ij} = 2\alpha^2 \left[ \hat{S}_{ij} - \frac{1}{3} \hat{S}_{kk} \delta_{ij} \right] - \hat{m}_{ij},$$

$$L_{ij} = \widehat{u}_i \widehat{u}_j - \widehat{u}_i \widehat{u}_j - \frac{1}{3} \left( \widehat{u}_k \widehat{u}_k - \widehat{u}_k \widehat{u}_k \right) \delta_{ij},$$

$$m_{ij} = 2|\overline{S}| \left[ \overline{S}_{ij} - \frac{1}{3} \overline{S}_{kk} \delta_{ij} \right],$$

$$E_i = \widehat{u}_i \widehat{T} - \widehat{u}_i \widehat{T},$$

$$F_i = \alpha^2 \left| \widehat{S} \right| \widehat{B}_i - \left| \overline{S} \right| B_i, \text{ and } B_j = \frac{\partial \overline{T}}{\partial x_j}.$$

Here,  $\alpha = \widehat{\Delta} / \overline{\Delta}$  is chosen as 2 in the present calculation,  $\langle \cdot \rangle_S$  denotes a spatial averaging over the horizontal plane to remove the calculation oscillation [13].

At the bottom wall  $z = 0$ , no-slip velocity condition is imposed. Assuming the free surface being in the absence of significant surface deformation, the boundary conditions applied at  $z = 1$ , for a shear-free interface without deformation, are given as

$$\bar{w} = 0, \quad \frac{\partial \bar{u}}{\partial z} = \frac{\partial \bar{v}}{\partial z} = 0 \tag{6}$$

The flow and temperature fields are assumed to be statistically homogeneous in the streamwise and spanwise directions. Thus, periodic boundary conditions are employed in both the directions. Two different constant temperatures, i.e.,  $T_F = 0.5$  and  $T_B = -0.5$ , are imposed on the free surface and the wall, respectively. Heat transfer computation is started after the flow field has statistically reached a fully developed turbulent state. Initial temperature field is set to be a linear distribution along the  $z$ -direction and homogeneous in the horizontal plane.

### 3. Numerical methods

To perform LES calculation, a fractional-step method proposed by Verzicco and Orlandi [26] is employed to solve Eqs. (1)–(3). Spatial derivatives are discretized by a second order central difference. Time advancement is carried out by the semi-implicit scheme using the Crank–Nicholson scheme for the viscous terms and the

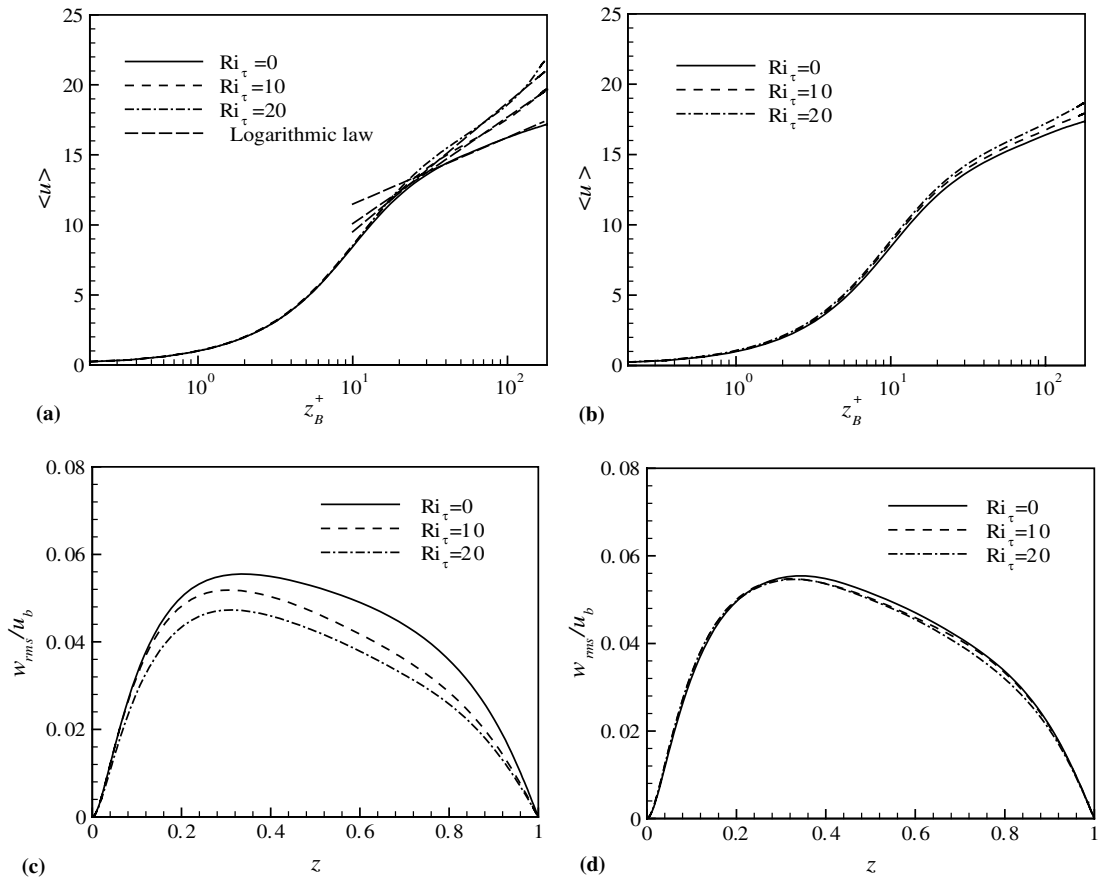


Fig. 1. Mean streamwise velocity at  $Pr = 1$  (a) and 100 (b) and the vertical velocity fluctuation normalized by the bulk-mean velocity at  $Pr = 1$  (c) and 100 (d).

three-stage Runge–Kutta scheme for the convective terms. The discretized formulation was described in detail by Verzicco and Orlandi [26].

In this study, the size of computational domain is  $4\pi\delta \times 3\pi\delta/2 \times \delta$  with the corresponding grid number  $128 \times 96 \times 96$  in the streamwise, spanwise and vertical directions, respectively. The domain size is chosen such that two-point correlations in both the streamwise and spanwise directions are negligibly small. The grid independence of the present calculation has been ensured for every simulation. The grid is uniform along the streamwise and spanwise directions. In the vertical direction, to increase the grid resolution near the free surface and the wall, the mesh is stretched with a transformation used in [27], so that the grid distribution is sufficient to resolve the viscous sublayer and diffusive sublayer near the boundaries [18,27].

The present computational LES code has been verified extensively in our previous work [18,19,27–29]. It can be ensured that our calculation is reliable for the prediction of statistical quantities of turbulent flow and heat transfer for thermally stratified turbulent flows.

#### 4. Results and discussion

##### 4.1. Velocity statistics

The buoyancy force in thermally stratified turbulent channel flow has a significant influence on the vertical turbulent transport and internal energy conversion between turbulent kinetic energy and turbulent potential energy. The velocity and temperature fields are coupled and affected each other. To exhibit the effect of  $Ri_\tau$  on the velocity statistics at different  $Pr$  numbers, Fig. 1a and b shows the mean streamwise velocity versus  $z_B^+$ , defined as  $z_B^+ = zu_c/v$ , for several  $Ri_\tau$  numbers at  $Pr = 1$  and 100. As shown in Fig. 1a for  $Pr = 1$ , in the sublayer,  $z_B^+ < 10$ , the results follow the linear law quite well. In the region of  $z_B^+ > 20$ , as  $Ri_\tau$  increases from 0 to 20, the flow speeds up. Clearly, the bulk mean velocity  $u_b$  increases with the increase of  $Ri_\tau$  although the friction velocity on the wall is not changed. This is evidence that the turbulent boundary layer appears the tendency of relaminarization in stably stratified flow, which is consistent with the results predicted for stably stratified turbulent two-walled channel flows with  $Pr = 0.71$  [30,31]. Furthermore, to explore the influence of  $Pr$  on the mean velocity, as shown in Fig. 1b for  $Pr = 100$ , the mean velocity profiles for several  $Ri_\tau$  numbers, unlike the case of  $Pr = 1$  in Fig. 1a, are nearly similar with each other. It is reasonably predicted that the effect of  $Ri_\tau$  on the mean velocity is somewhat negligible in weakly stratified high-Prandtl number turbulent flows.

As indicated by Garg et al. [30] and Arya [32], a logarithmic region in weakly stratified boundary layer still

appears. By examining the velocity profiles in Fig. 1a, they have a logarithmic form,

$$\langle u^+ \rangle = (1/K) \ln z_B^+ + B \tag{7a}$$

where  $K$  and  $B$  represent the von Kármán constant and the additive constant in the log law of the velocity profile, respectively. Both  $K$  and  $B$  depend on  $Ri_\tau$  and are obtained from Fig. 1a. As shown in Fig. 2,  $K$  and  $B$  decrease with the increase of  $Ri_\tau$ . According to Prandtl's mixing length model [33], the turbulent eddy viscosity in the logarithmic layer is  $\nu_T \sim l_m |d\langle \bar{u} \rangle / dz|^2$ , where  $l_m \approx Kz$  is the mixing length. Under stable stratification, turbulence intensities are suppressed and the vertical length scale decreases, which is accounted for by decreasing  $K$ .

Fig. 1c and d shows the vertical velocity fluctuation normalized by the bulk mean velocity  $u_b$  at  $Pr = 1$  and 100. The turbulence intensities considerably decrease

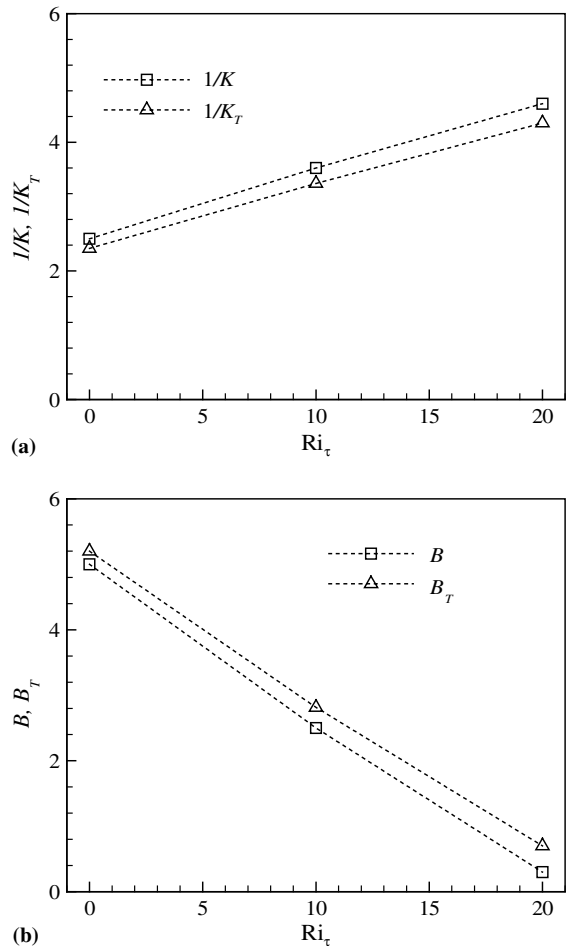


Fig. 2. The von Kármán constant  $K$  and  $K_T$  (a) and the additive constant  $B$  and  $B_T$  (b) in the log law of the velocity and temperature profiles versus the Richardson number at  $Pr = 1$ .

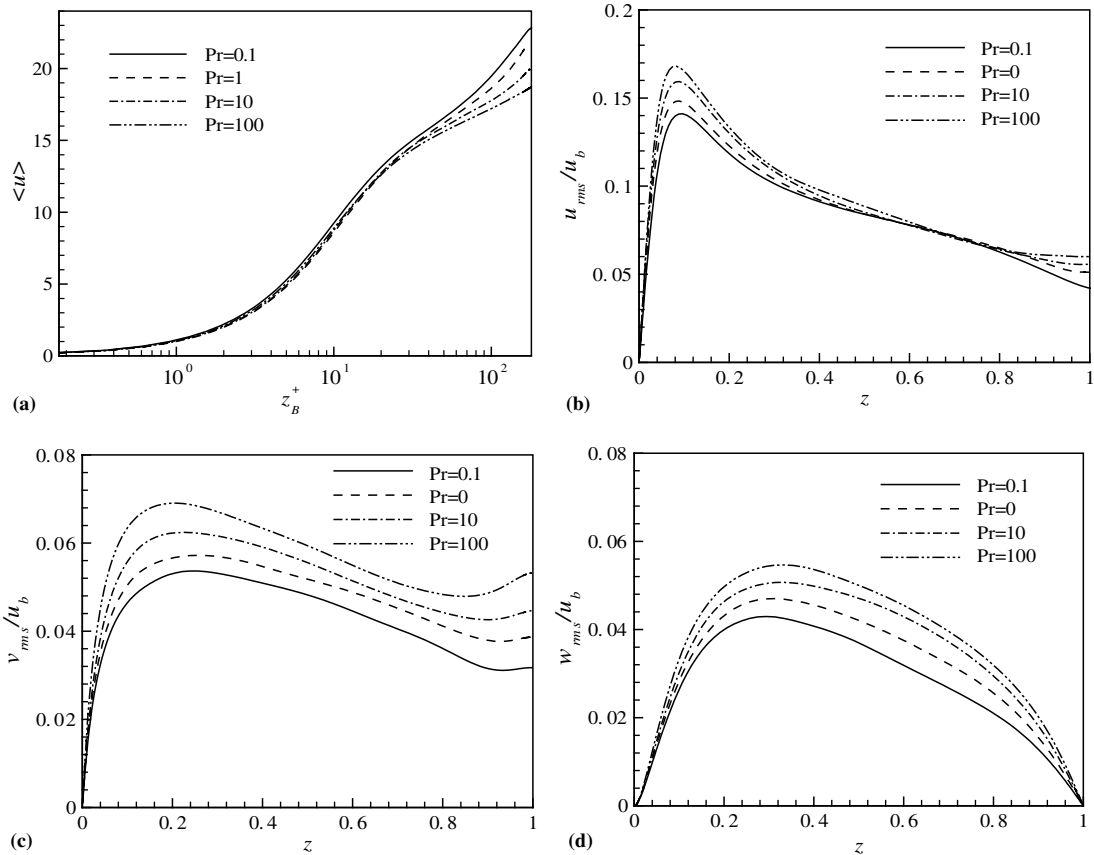


Fig. 3. Mean velocity and turbulence intensities normalized by the bulk-mean velocity at  $Ri_\tau = 20$ : (a) mean streamwise velocity; (b) streamwise velocity fluctuation; (c) spanwise velocity fluctuation; (d) vertical velocity fluctuation.

for low- to moderate-Prandtl number (e.g.,  $Pr = 1$ ) turbulent flows due to stable stratification. The tendency of re-laminarization of turbulent boundary layer is characterized by the decrease of the turbulence intensities. However, as shown in Fig. 1d for high-Prandtl number flow, the stratification effect on the turbulence intensities is insignificant.

To exhibit the effect of  $Pr$  on turbulence statistics, Fig. 3 shows the mean velocity and turbulence intensities for several  $Pr$  numbers at  $Ri_\tau = 20$ . As  $Pr$  decreases, the flow speeds up and the bulk mean velocity increases. Correspondingly, the turbulence intensities decrease. Thus, the effect of decreased  $Pr$  is to enhance the relaminarizing effect of stable stratification. It is also disclosed that the effect of  $Pr$  has a considerable influence on turbulence statistics. Métais and Herring [34] performed a DNS of freely evolving stably stratified turbulence with  $Pr = 1$  and well compared their DNS data with experimental data for  $Pr = 200$  [35]. Then, they argued that the large-scale structures are similar in both the DNS and the experiment. Based on our calculated results, however, it is verified that the effect of  $Pr$  plays an

important role in the dynamics of turbulence in thermally stratified flows.

#### 4.2. Temperature and thermal statistics

Fig. 4a and b shows the mean temperature profiles for different  $Ri_\tau$  numbers at  $Pr = 1$  and 100, respectively, where  $\langle T^+ \rangle$  is defined as  $\langle T^+ \rangle = [\langle \overline{T} \rangle - T_B] / T_\tau$  with  $T_\tau$  being the friction temperature at the wall,  $T_\tau = (\kappa / u_\tau) |\partial \langle \overline{T} \rangle / \partial z|_{z=0}$ . Similar to the mean velocity distribution in Fig. 1a and b, there exists a buffer layer followed by a logarithmic region in the mean temperature profile;  $\langle T^+ \rangle$  behaves as

$$\langle T^+ \rangle = (1/K_T) \ln z_B^+ + B_T \tag{7b}$$

where  $K_T$  and  $B_T$  represent the von Kármán constant and the additive constant in the log law of the mean temperature profile. It is confirmed that  $K_T$  and  $B_T$  depend on  $Ri_\tau$ . For unstratified turbulent flow, i.e.,  $Ri_\tau = 0$ , Kader and Yaglom [36] found  $1/K_T = 2.12$  approximately, which is consistent with our predicted data shown in Fig. 2, while Kader [37] gave an empirical expression

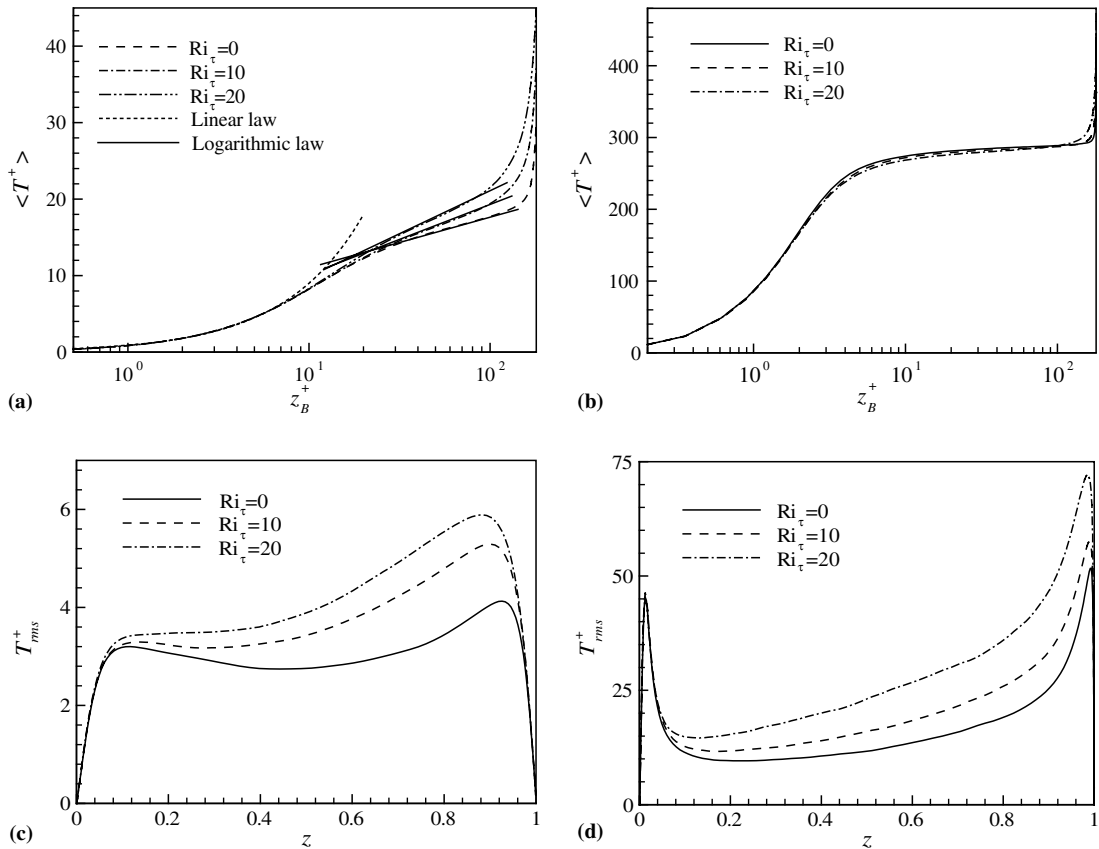


Fig. 4. Mean temperature normalized by the friction temperature at  $Pr = 1$  (a) and 100 (b) and its fluctuation at  $Pr = 1$  (c) and 100 (d).

for the function  $B_T$  that describes the experimental results in the logarithmic region of the fully turbulent boundary layer. Based on the temperature profiles in Fig. 4a for  $Pr = 1$ , as  $Ri_\tau$  increases, both  $K_T$  and  $B_T$  decrease in Fig. 2.

Similar to the behavior of the mean velocity profiles (Fig. 1a and b), as shown in Fig. 4b for  $Pr = 100$ , the change of the mean temperature profile due to the stratification effect is also nearly negligible. However, as shown in Fig. 4c and d for the profiles of the temperature fluctuation ( $T_{rms}^+$ ) normalized by  $T_\tau$ , it is evident that the influence of  $Ri_\tau$  on  $T_{rms}^+$  is obvious for both  $Pr = 1$  and 100, in particular near the free surface. Meanwhile, the local maximum of  $T_{rms}^+$  near the free surface is higher than that near the bottom wall; this phenomenon is consistent with previous work [12,27]. As  $Pr$  increases, the peak value of  $T_{rms}^+$  near the free surface (or the wall) increases, and their positions shift towards the free surface (or the wall). As  $Ri_\tau$  increases, the peak value of  $T_{rms}^+$  near the free surface increases and its position moves away from the free surface. Due to stable stratification effect, when  $Ri_\tau$  increases, the velocity fluctuations (Fig. 1) decrease and the temperature fluctu-

ation (Fig. 4) increases. The mechanism can be explained by internal energy conversion between the turbulent kinetic energy and turbulent potential energy that is related to the square of the temperature fluctuation [30].

To reveal further the effect of  $Pr$  on the mean temperature, Fig. 5 shows the mean temperature profiles plotted by both normalized scales at  $Ri_\tau = 20$ . To exhibit the global behavior of the mean temperature, as shown in Fig. 5a, it is noted that the diffusive sublayer becomes thinner and thinner with the increase of  $Pr$ . Shaw and Hanratty [38] investigated experimentally and theoretically on fully developed turbulent wall flow with passive heat transfer, and proposed that the diffusive sublayer thickness at different  $Pr$  numbers was related approximately to the  $Pr^{-1/3}$  law predicted by theoretical analysis and to the  $Pr^{-0.3}$  law by experiment. From Fig. 5, it is identified that the values of the diffusive sublayer thickness near the bottom wall for different  $Pr$  numbers are still very close to those laws in weakly stratified turbulent flows. By checking the profiles in Fig. 5a, it is also noted that the values of the diffusive sublayer thickness near the free surface are related to the law  $Pr^{-1/2}$

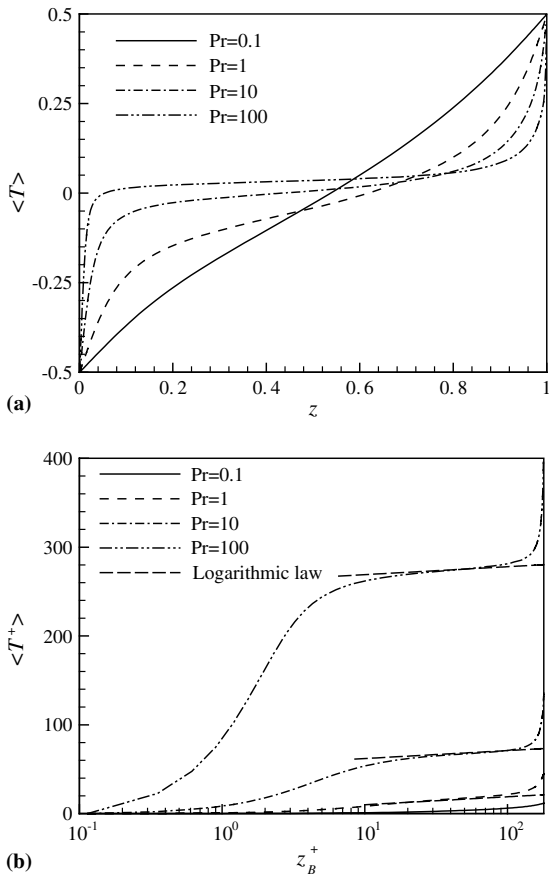


Fig. 5. Profiles of the mean temperature at  $Ri_\tau = 20$ : (a) over the channel; (b) temperature normalized by the friction temperature near the wall.

approximately, which is determined based on standard surface renewal model [5]. This behavior can be confirmed further by the variation of turbulent heat transfer coefficient (or the Nusselt number) versus  $Pr$  at the free surface in the following.

In Fig. 5b, the  $z_B^+$ -logarithmic plots of the mean temperature profile near the wall may be nearly parallel for different  $Pr$  numbers. The slope of  $1/K_T$  in Eq. (7b) varies with  $Ri_\tau$  (Fig. 2); however, it is approximately constant for several  $Pr$  numbers, almost independent of  $Pr$ , which is consistent with the findings for unstratified flows [18,27,39].

Here, we try to explain why the stratification effect on the velocity statistics is negligibly small in weakly stratified high-Prandtl number turbulent flow. The primary parameter associated with stratification in shear flows is the gradient Richardson number,  $Ri_g = N^2/S^2$ , where  $N$  is the Brunt–Väisälä frequency and  $S$  is the mean shear rate, which appears to be the important local determinant of buoyancy effects [30,31]. The buoyancy flux in stratified boundary layer is boundary-driven with

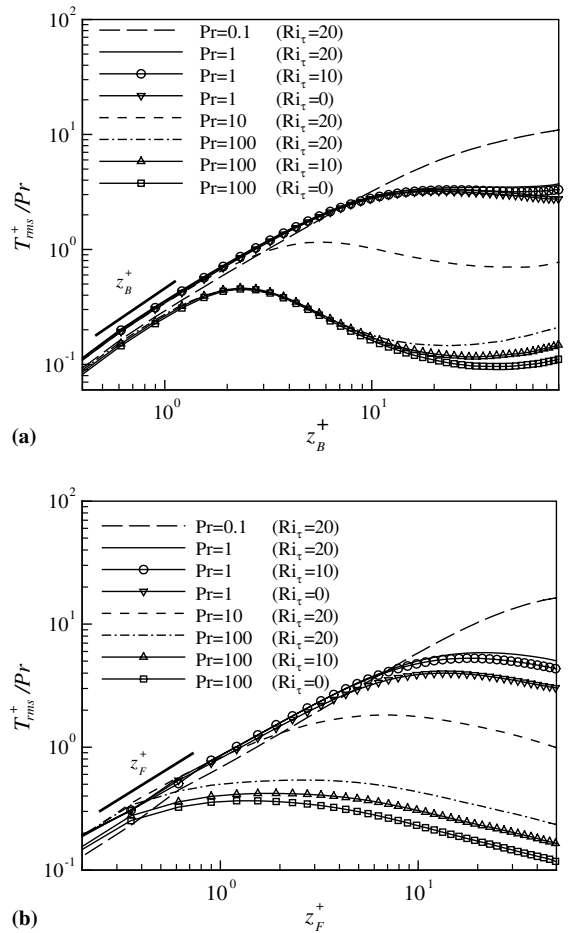


Fig. 6. Profiles of the temperature fluctuations near the wall (a) and near the free surface (b).

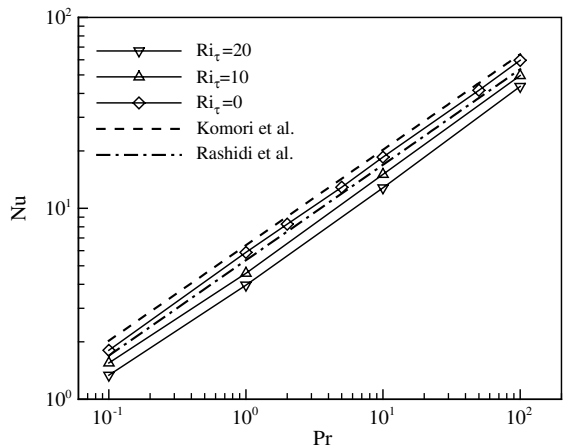


Fig. 7. Nusselt number versus the Prandtl number for both unstratified and stratified flows and the comparison with the corrections proposed by Komori et al. [2] and Rashidi et al. [5].

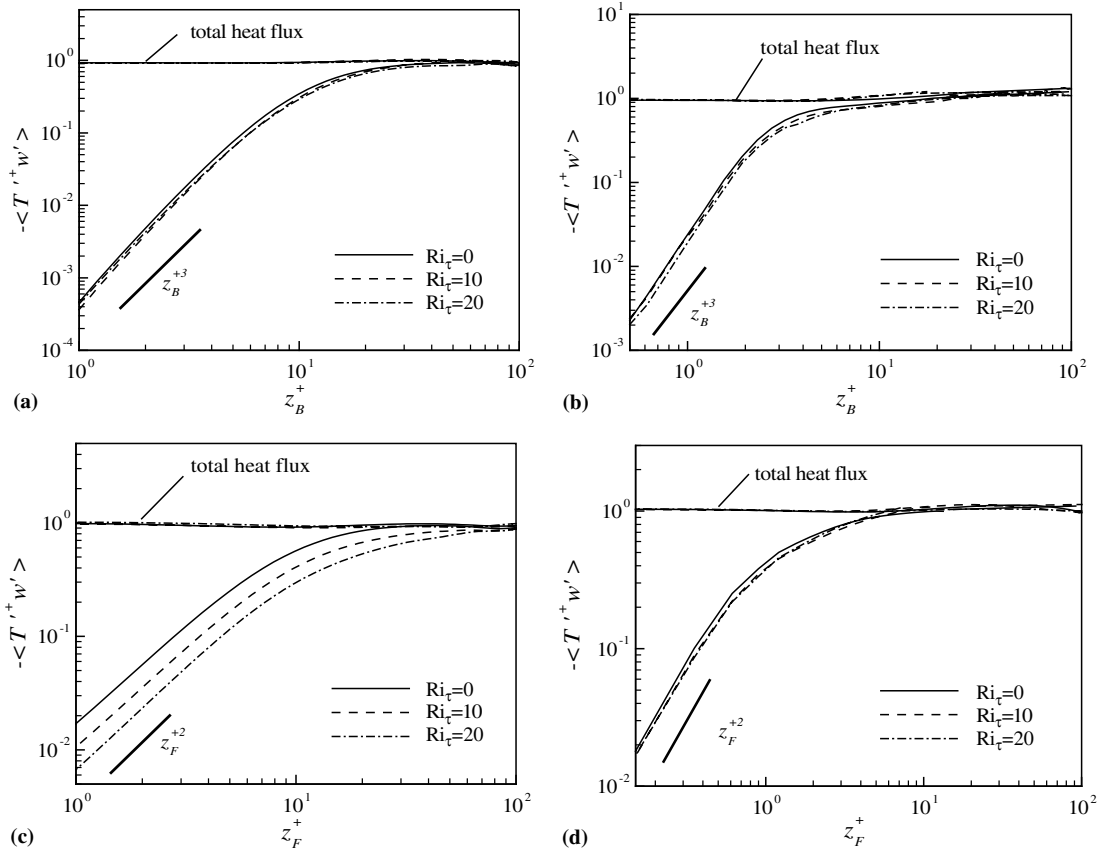


Fig. 8. Profiles of the mean vertical turbulent heat fluxes near the wall for  $Pr = 1$  (a) and 100 (b) and near the free surface for  $Pr = 1$  (c) and 100 (d).

the turbulence originating near the wall where  $Ri_g$  is small. Then, passing to the outer boundary region, the local values of  $Ri_g$  are large for low- to moderate-Prandtl number because a significant temperature gradient exists in the region outside the sublayer (Fig. 5a), but still small for large-Prandtl number because the temperature is nearly constant over the most core region of the channel. Thus, it is reasonable to predict the buoyancy effect has little influence on the velocity statistics in weakly stratified high-Prandtl number turbulent flows.

To elucidate the effects of  $Pr$  and  $Ri_\tau$  on the temperature fluctuation, Fig. 6 shows the profiles of the temperature fluctuation plotted logarithmically to emphasize the behaviors near the wall and the free surface for some typical parameters. In the wall (or free surface) vicinity, the temperature fluctuation can be expanded, in terms of  $z_B^+$  (or  $z_F^+ = (1 - z)u_\tau/\nu$ ), as [40],

$$T_{rms}^+ = a_{B1}z_B^+ + a_{B2}z_B^{+2} + \dots \quad \text{near the wall} \quad (8a)$$

$$T_{rms}^+ = a_{F1}z_F^+ + a_{F2}z_F^{+2} + \dots \quad \text{near the free surface} \quad (8b)$$

Usually, the expansion coefficients are dependent of the relevant parameters (e.g.,  $Ri_\tau$ ,  $Re_\tau$ ). As shown in Fig. 6, the expansions of Eq. (8) can be confirmed based on the agreement of the leading terms in Eq. (8) with the profiles in the regions of the wall and the free surface.

The Nusselt number is an important parameter relevant to the heat transfer coefficient and, at the free surface, is defined as

$$Nu = \frac{q_F \delta}{k \Delta T} \quad (9)$$

where  $q_F$  represents the averaged heat flux through the free surface, and  $k$  is the thermal conductivity. Fig. 7 shows the Nusselt number versus  $Pr$ . It is confirmed that the distribution of  $Nu$  is well related to the law  $Pr^{1/2}$  for unstratified ( $Ri_\tau = 0$ ) and stratified ( $Ri_\tau = 10, 20$ ) flows and decreases with the increase of  $Ri_\tau$  for the same  $Pr$ . This behavior is quite rational because stable stratification dissociates the surface-renewal motions and restrains the heat transfer at the free surface.

To validate the present prediction, we compare our results with the gas flux measurements of Komori et al. [2] and the empirical correlation developed by

Rashidi et al. [5]. They correlated their experimental results with the subsurface hydrodynamics with the aid of the surface renewal approximation. The correlations can be normalized using only the Reynolds and Prandtl numbers as

$$NuPr^{-1/2} = 4.21 \times 10^{-3} Re_m^{0.927} \quad (\text{Komori et al. [2]}) \tag{10a}$$

$$NuPr^{-1/2} = 3.22 \times 10^{-3} Re_m^{0.938} \quad (\text{Rashidi et al. [5]}) \tag{10b}$$

where  $Re_m$  is the Reynolds number based on the bulk mean velocity  $u_b$ . Based on our data at  $Ri_\tau = 0$ ,  $Re_m$  is calculated as 2695 approximately. Fig. 7 depicts comparisons of  $Nu$  predicted by the present LES together with the empirical correlations expressed by Eq. (10). The results predicted by the present calculation at  $Ri_\tau = 0$  are in a reasonable agreement with correlations given by Eq. (10) and lay between them. Despite somewhat difference between the present prediction and the correlations, we consider the present  $Nu$  prediction acceptable since, to make a fair comparison, unavoi-

able experimental errors must be considered. Further, the comparisons in Fig. 7 also indicate clearly that the correlations in Eq. (10) must be modified to be feasible for the prediction of  $Nu$  in stably stratified flows for different  $Ri_\tau$  numbers.

Fig. 8 shows the resolved vertical turbulent heat fluxes near the free surface and the wall at  $Pr = 1$  and 100. Note that the temperature fluctuation in the heat fluxes is normalized by the friction temperature. In Fig. 8a and c for  $Pr = 1$ , as  $Ri_\tau$  increases, the vertical turbulent heat fluxes (i.e.,  $-\langle w'T'^+ \rangle$ ) decreases obviously, especially near the free surface. However, as shown in Fig. 8b and d, the stratification effect on the turbulent heat fluxes is small for high-Prandtl number flow; this behavior is consistent with the change of turbulence statistics described earlier.

Furthermore, considering the wall boundary and the shear free conditions, the turbulent heat flux  $-\langle w'T'^+ \rangle$  can be expanded into power series of  $z_B^+$  and  $z_F^+$  in the vicinities of the wall and the free surface,

$$-\langle w'T'^+ \rangle = a_1 z_B^{+3} + a_2 z_B^{+4} + \dots \quad \text{near the wall} \tag{11a}$$

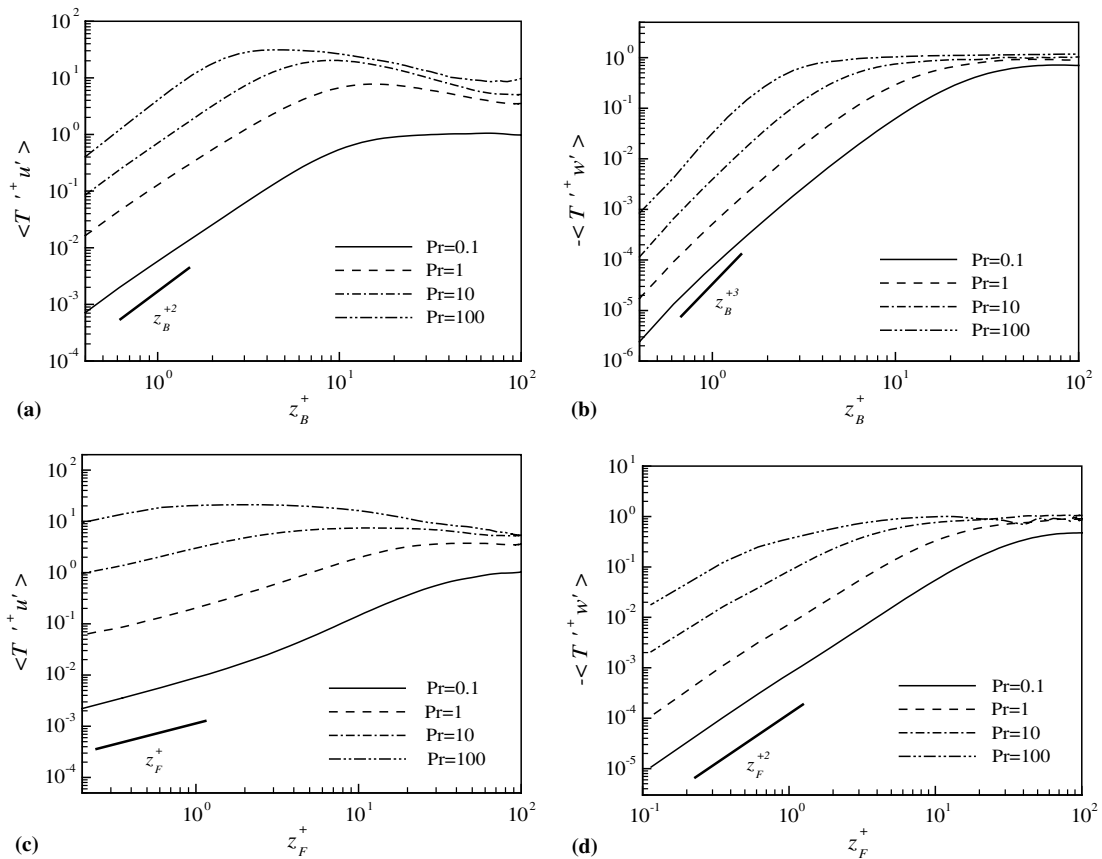


Fig. 9. Profiles of the streamwise (a) and vertical (b) turbulent heat fluxes near the wall as well as the streamwise (c) and vertical (d) turbulent heat fluxes near the free surface at  $Ri_\tau = 20$ .

$$-\langle w'T'^+ \rangle = b_1 z_F^{+2} + b_2 z_F^{+3} + \dots \quad \text{near the free surface} \quad (11b)$$

Then, both curves of the square and cubic laws with the vertical distance  $z_F^+$  and  $z_B^+$  are plotted in Fig. 8 with logarithmic scales to illustrate the first terms in Eq. (11). As expected, the turbulent heat fluxes agree well with the leading terms in Eq. (11). The total heat flux, which is the sum of the wall-normal turbulent and molecular heat flux, is also depicted in Fig. 8. As expected, based on theoretical analysis, it is seen that the normalized total heat flux equals nearly to unity under the temperature boundary conditions used here. This behavior also ensures that the temperature field is fully developed and the present calculation is accurately reliable.

Further, to elucidate the effect of  $Pr$  on the turbulent heat fluxes, Fig. 9 shows the streamwise and vertical turbulent heat fluxes near the wall and the free surface for

several  $Pr$  numbers at  $Ri_\tau = 20$ . As  $Pr$  increases, the turbulent heat fluxes become increasingly significant in the near regions of the free surface and the wall.

Similarly, the streamwise turbulent heat flux  $\langle u'T'^+ \rangle$  can be also expressed as power series of  $z_B^+$  and  $z_F^+$  near the boundaries,

$$\langle u'T'^+ \rangle = c_1 z_B^{+2} + c_2 z_B^{+3} + \dots \quad \text{near the wall} \quad (12a)$$

$$\langle u'T'^+ \rangle = d_1 z_F^{+2} + d_2 z_F^{+3} + \dots \quad \text{near the free surface} \quad (12b)$$

Fig. 9 also depicts the curves to exhibit the first terms in Eqs. (11) and (12). Although the influence of the stratification effect appears, the turbulent heat fluxes in the streamwise and vertical directions are still in good agreement with the leading terms in Eqs. (11) and (12) near the boundaries.

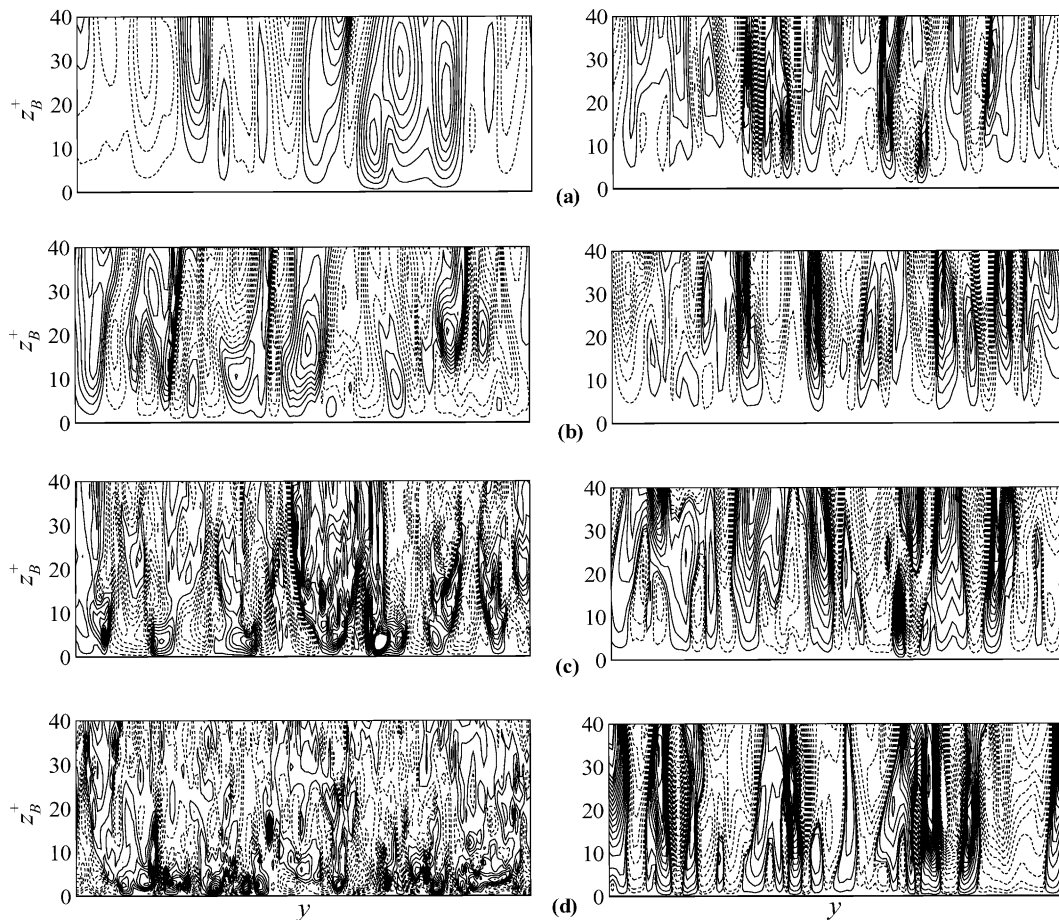


Fig. 10. Contours of the instantaneous temperature fluctuation (left column) and vertical velocity fluctuation (right column) in a cross plane ( $y, z_B^+$ ) near the wall for  $Ri_\tau = 20$ : (a)  $Pr = 0.1$ ; (b) 1; (c) 10; and (d) 100. Here, solid lines represent positive values and dashed lines negative values. Increments of the temperature and vertical velocity fluctuations are 0.02 and 0.2, respectively.

#### 4.3. Structures of the temperature and velocity fluctuation

The stratification effect on the turbulent structures has been extensively investigated in previous work [25,30,31]. Here, the structures of the temperature and velocity fluctuation near the wall and the free surface are briefly analyzed to exhibit the influence of the Prandtl number.

Fig. 10 shows the contours of the instantaneous temperature and vertical velocity fluctuation near the wall in a cross plane  $(y, z_F^+)$  for  $Ri_\tau = 20$ ,  $Pr = 0.1, 1, 10$  and  $100$ . The organized streaks of the high- and low-temperature fluctuation exhibit the coherent structures due to the succession of ejection and sweeping events. It is noted that smaller scale structures near the wall occur for higher  $Pr$  number. The scale of temperature fluctuation decreases with the increase of  $Pr$  in a manner inversely proportional to  $Pr^{1/2}$  [41]. The vertical size of the closed contours clearly shows that the heat transfer takes place

in a very thin region for high-Prandtl number flow. Because weak stratification effect is considered here, the organized streak structures of the vertical velocity fluctuation for several  $Pr$  numbers are nearly similar to each other. The velocity fluctuation appears somewhat close to the wall at high-Prandtl number.

Correspondingly, the instantaneous temperature and vertical velocity fluctuations near the free surface in a cross plane  $(y, z_F^+)$  are also shown in Fig. 11. It is evident that the structure scale in the temperature fluctuation decreases with the increase of  $Pr$ . These structures spread over the region near the free surface; it is because a large fraction of surface renewal events originate from the buffer region of the wall boundary layer [5–7]. Meanwhile, it is noted that the vertical velocity fluctuation occurs obviously close to the free surface at high-Prandtl number because the velocity is affected by thermal effect with thinner diffusive sublayer for higher Prandtl number.

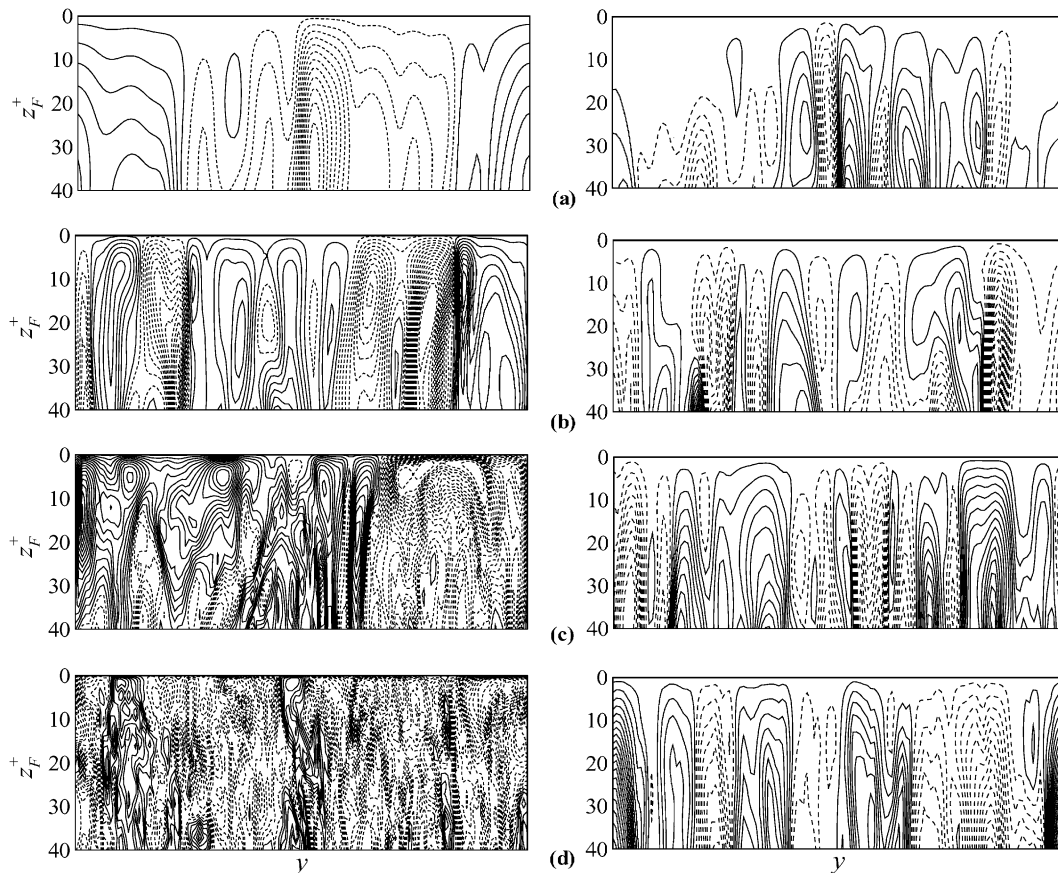


Fig. 11. Contours of the instantaneous temperature fluctuation (left column) and vertical velocity fluctuation (right column) in a cross plane  $(y, z_F^+)$  near the free surface for  $Ri_\tau = 20$ : (a)  $Pr = 0.1$ ; (b) 1; (c) 10; and (d) 100. Here, increments of the temperature and vertical velocity fluctuations are 0.02 and 0.1, respectively.

Based on the patterns of the velocity and temperature fluctuations near the boundaries for different  $Ri_\tau$  numbers (not shown here), it is noted that the formation of streaks near the wall is suppressed with the increase of  $Ri_\tau$ . This behavior is also confirmed in stably stratified turbulent two-walled channel flows [30,31] as well as is closely related to the reduction of the friction coefficient at the wall [42] and to the decrease of turbulent heat flux at the free surface as shown in Fig. 7. The dissociation of the streaky structures in the near wall region also means that the frequency of the bursting eddies decreases in stably stratified turbulence. Meanwhile, according to Komori et al. [2], about 90% of bursting eddies generated in the near wall turbulent boundary layer evolve the surface-renewal motions. Thus, the frequency of the surface-renewal motions decreases due to the effect of stable stratification.

Further, the temperature fluctuation patterns in a plane parallel to the wall at  $z_B^+ = 0.35$  (near the wall)

and  $z_F^+ = 0.35$  (near the free surface) for different  $Pr$  numbers are shown in Fig. 12, where the high- and low-temperature streaks are visualized. The patterns clearly illustrate the evolution of temperature fluctuation with absent and dense streaky structures for different  $Pr$  numbers; this behavior is consistent with the profiles of the temperature fluctuation in Fig. 6. In the near wall region, absent streaky structures appear at low  $Pr$  number, e.g.,  $Pr = 0.1$  and 1 in Fig. 12a and b, and fairly dense and long streaky structures occur at high  $Pr$  number, e.g.,  $Pr = 10$  and 100 in Fig. 12c and d. As discussed above, because the surface renewal events mainly originate from the buffer region of the wall, it is reasonably observed that the temperature fluctuation with the absent and dense streaky structures near the free surface well corresponds to that near the wall. Thus, the temperature fluctuation near the free surface increases with the increase of  $Pr$ , which is reasonably related to the behavior of the Nusselt number at the free surface versus  $Pr$  as shown in Fig. 7.

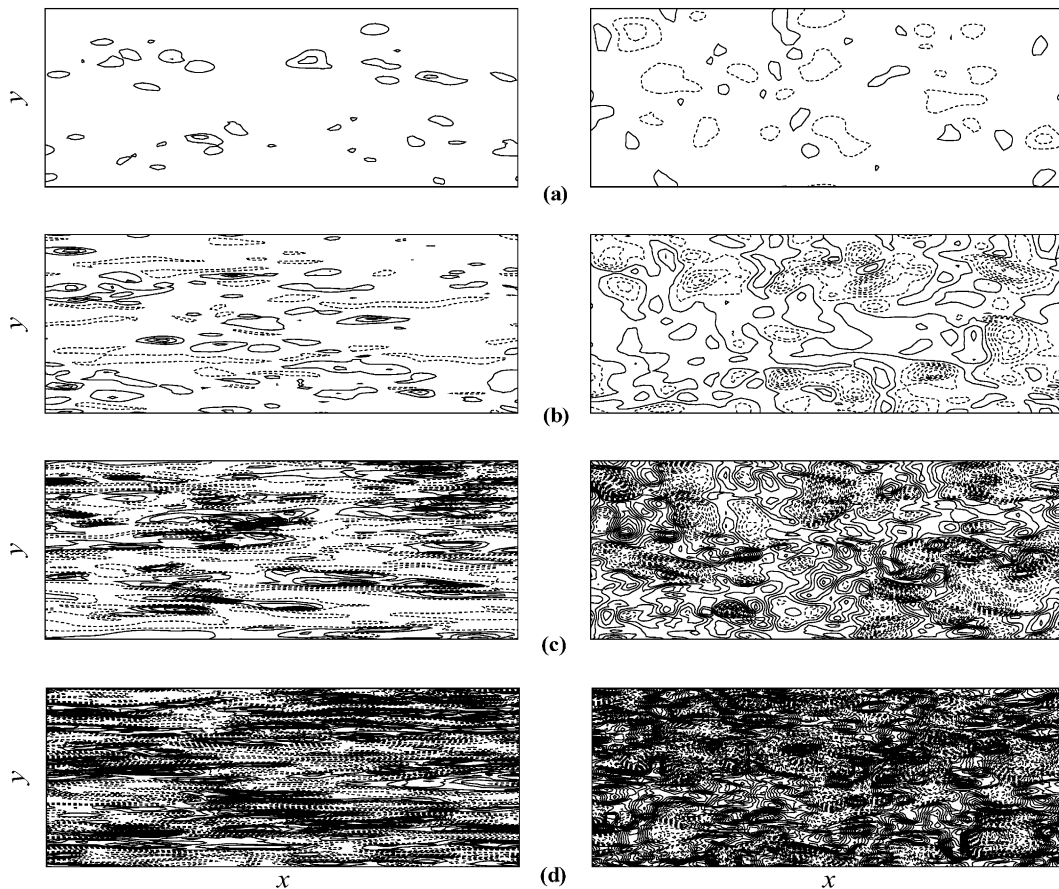


Fig. 12. Contours of the instantaneous temperature fluctuation near the wall at  $z_B^+ = 0.35$  (left column) and near the free surface at  $z_F^+ = 0.35$  (right column) for  $Ri_\tau = 20$ : (a)  $Pr = 0.1$ ; (b) 1; (c) 10; and (d) 100. Here, increment of the temperature fluctuation is 0.005.

## 5. Concluding remarks

Large eddy simulation of thermally stratified turbulent open channel flow is carried out to reveal the effects of  $Ri_\tau$  and  $Pr$  on the characteristics of turbulent flow, heat transfer, and large-scale motions in weakly stratified turbulence. The profiles of the mean velocity and temperature have been examined for several  $Ri_\tau$  and  $Pr$  numbers; there exists a buffer layer followed by a logarithmic region in the velocity and temperature profiles. Both the von Kármán constant and the additive constant in the log law of these profiles decrease with the increase of  $Ri_\tau$ . However, the plots of the mean temperature profiles in the logarithmic region may be nearly parallel for different  $Pr$  numbers, and thus their slopes are almost independent of  $Pr$  number. It is found that the stratification effect has little influence on the velocity statistics in weakly stratified high-Prandtl number turbulent flow, although the effect is significant on turbulent behaviors for low- to moderate-Prandtl number turbulent flows. Meanwhile, as  $Pr$  decreases, the flow speeds up and the bulk mean velocity increases and the turbulence intensities decrease. The effect of decreased  $Pr$  is thus to enhance the relaminarizing effect of stable stratification. Under stable stratification influence, as  $Ri_\tau$  increases, the velocity fluctuations decrease and the temperature fluctuation increases; this behavior is relevant to the mechanism of internal energy conversion between the turbulent kinetic energy and the potential energy.

The Nusselt number at the free surface predicted by the present LES is well consistent with the law  $Pr^{1/2}$  for both unstratified and stratified flows. The Nusselt number decreases with the increase of  $Ri_\tau$ ; it is because stable stratification dissociates the surface-renewal motions and restrains the heat transfer at the free surface. Based on our calculated results, it is suggested that the correlations related to the Nusselt number with the Reynolds and Prandtl numbers, proposed by Komori et al. [2] and Rashidi et al. [5], must be modified for stratified turbulent flow. The turbulent heat fluxes for unstratified and stratified flows are in good agreement with some local features expressed by analytical predictions near the wall and the free surface.

Based on the structures of the instantaneous temperature and velocity fluctuations, it is revealed that the turbulent heat transfer takes place in a very thin region at high-Prandtl number and only the smallest structures subsisting very close to the wall are involved in the heat transfer process. The effect of  $Pr$  on the organized streak structures of the velocity fluctuations is somewhat not remarkable for weakly stratified turbulent flow. However, the influence of  $Pr$  on the structures of the temperature fluctuations is significant.

## Acknowledgments

This work was supported by the National Natural Science Foundation of China (no. 90405007, 10125210), the China NKBRF Project (no. 2001CB409600), Specialized Research Fund for the Doctoral Program of Higher Education (no. 20020358013), and the Hundred Talents Programme of the Chinese Academy of Sciences. The authors are grateful for valuable comments of the referees.

## References

- [1] H. Nakagawa, I. Nezu, Structure of space-time correlations of bursting phenomena in open-channel flow, *J. Fluid Mech.* 104 (1981) 1–43.
- [2] S. Komori, R. Nagaosa, Y. Murakami, Mass transfer into a turbulent liquid across the zero-shear gas–liquid interface, *AIChE J.* 36 (1990) 957–960.
- [3] S. Komori, R. Nagaosa, Y. Muramami, Turbulence structure and mass transfer across a sheared air–water interface in wind driven turbulence, *J. Fluid Mech.* 249 (1993) 161–183.
- [4] S. Kumar, R. Gupta, S. Banerjee, An experimental investigation of the characteristics of free-surface turbulence in channel flow, *Phys. Fluids* 10 (1998) 437–456.
- [5] M. Rashidi, G. Hetstroni, S. Banerjee, Mechanisms of heat and mass transport at gas–liquid interfaces, *Int. J. Heat Mass Transfer* 34 (1991) 1799–1805.
- [6] M. Rashidi, Burst-interface interactions in free surface turbulent flows, *Phys. Fluids* 9 (1997) 3485–3501.
- [7] S. Komori, R. Nagaosa, Y. Murakami, S. Chiba, K. Ishii, K. Kuwahara, Direct numerical simulation of three-dimensional open-channel flow with zero-shear gas–liquid interface, *Phys. Fluids* 5 (1993) 115–125.
- [8] Y. Pan, S. Banerjee, A numerical study of free-surface turbulence in channel flow, *Phys. Fluids* 7 (1995) 1649–1664.
- [9] P. Lombardi, V. De Angelis, S. Banerjee, Direct numerical simulation of near-interface turbulence in coupled gas–liquid flow, *Phys. Fluids* 8 (1996) 1643–1665.
- [10] R. Nagaosa, R.A. Handler, Statistical analysis of coherent vortices near a free surface in a fully developed turbulence, *Phys. Fluids* 15 (2003) 375–394.
- [11] R. Nagaosa, Direct numerical simulation of vortex structures and turbulent scalar transfer across a free surface in a fully developed turbulence, *Phys. Fluids* 11 (1999) 1581–1595.
- [12] R.A. Handler, J.R. Saylor, R.I. Leighton, A.L. Rovelstad, Transport of a passive scalar at a shear-free boundary in fully developed turbulent open channel flow, *Phys. Fluids* 11 (1999) 2607–2625.
- [13] M. Germano, U. Piomelli, P. Moin, W. Cabot, A dynamic subgrid-scale eddy viscosity model, *Phys. Fluids* 3 (1991) 1760–1765.
- [14] J. Smagorinsky, General circulation experiments with the primitive equations. I. The basic experiment, *Mon. Weather Rev.* 91 (1963) 99–165.

- [15] P. Moin, K. Squires, W. Cabot, S. Lee, A dynamic subgrid-scale model for compressible turbulent and scalar transport, *Phys. Fluids* 3 (1991) 2746–2757.
- [16] Y. Zang, R.L. Street, J.R. Koseff, A dynamic mixed subgrid-scale model and its application to turbulent recirculating flows, *Phys. Fluids* 5 (1993) 3186–3196.
- [17] I. Calmet, J. Magnaudet, Large-eddy simulation of high-Schmidt number mass transfer in a turbulent channel flow, *Phys. Fluids* 9 (1997) 438–455.
- [18] Y.H. Dong, X.Y. Lu, L.X. Zhuang, Large eddy simulation of turbulent channel flow with mass transfer at high-Schmidt numbers, *Int. J. Heat Mass Transfer* 46 (2003) 1529–1539.
- [19] L. Wang, X.Y. Lu, An investigation of turbulent oscillatory heat transfer in channel flows by large eddy simulation, *Int. J. Heat Mass Transfer* 47 (2004) 2161–2172.
- [20] M.V. Salvetti, Y. Zang, R.L. Street, S. Banerjee, Large-eddy simulation of free-surface decaying turbulence with dynamic subgrid-scale models, *Phys. Fluids* 9 (1997) 2405–2419.
- [21] I. Calmet, J. Magnaudet, Statistical structure of high-Reynolds-number turbulence close to the free surface of an open-channel flow, *J. Fluid Mech.* 474 (2003) 355–378.
- [22] S. Komori, H. Ueda, F. Ogino, T. Mizushima, Turbulence structure in stably stratified open-channel flow, *J. Fluid Mech.* 130 (1983) 13–26.
- [23] T. Gerz, U. Schumann, S.E. Elgobashi, Direct numerical simulation of stratified homogeneous turbulent shear flows, *J. Fluid Mech.* 200 (1989) 563–594.
- [24] S.E. Holt, J.R. Koseff, J.H. Ferziger, A numerical study of the evolution and structure of homogeneous stably stratified sheared turbulence, *J. Fluid Mech.* 237 (1992) 499–539.
- [25] R. Nagaosa, T. Saito, Turbulence structure and scalar transfer in stratified free-surface flows, *AIChE J.* 43 (1997) 2393–2404.
- [26] R. Verzicco, P. Orlandi, A finite-difference scheme for three-dimensional incompressible flows in cylindrical coordinates, *J. Comput. Phys.* 123 (1996) 402–414.
- [27] L. Wang, Y.H. Dong, X.Y. Lu, An investigation of turbulent open channel flow with heat transfer by large eddy simulation, *Comput. Fluids* 34 (2005) 23–47.
- [28] Y.H. Dong, X.Y. Lu, Large eddy simulation of a thermally stratified turbulent channel flow with temperature oscillation on the wall, *Int. J. Heat Mass Transfer* 47 (2004) 2109–2122.
- [29] N.S. Liu, X.Y. Lu, Large eddy simulation of turbulent concentric annular channel flows, *Int. J. Numer. Methods Fluids* 45 (2004) 1317–1338.
- [30] R.P. Garg, J.H. Ferziger, S.G. Monismith, J.R. Koseff, Stably stratified turbulent channel flows. I. Stratification regimes and turbulence suppression mechanism, *Phys. Fluids* 12 (2001) 2569–2594.
- [31] V. Armenio, S. Sarkar, An investigation of stably-stratified turbulent channel flow using large eddy simulation, *J. Fluid Mech.* 459 (2002) 1–42.
- [32] S.P.S. Arya, Buoyancy effects in a horizontal flat-plate boundary layer, *J. Fluid Mech.* 68 (1975) 321–343.
- [33] W.M. Kays, M.E. Crawford, *Convective Heat and Mass Transfer*, McGraw-Hill, New York, 1987.
- [34] O. Métais, J.R. Herring, Numerical simulations of freely evolving turbulence in stably stratified fluids, *J. Fluid Mech.* 202 (1989) 117–148.
- [35] E.C. Itsweire, K.N. Helland, C.W. Van Atta, The evolution of grid-generated turbulence in a stably stratified fluid, *J. Fluid Mech.* 162 (1986) 299–338.
- [36] B.A. Kader, A.M. Yaglom, Heat and mass transfer laws for fully turbulent wall flows, *Int. J. Heat Mass Transfer* 15 (1972) 2329–2342.
- [37] B.A. Kader, Temperature and concentration profiles in fully turbulent boundary layers, *Int. J. Heat Mass Transfer* 24 (1981) 1541–1545.
- [38] D.A. Shaw, T.J. Hanratty, Turbulent mass transfer rates to a wall for large Schmidt number, *AIChE J.* 23 (1977) 28–35.
- [39] H. Kawamura, H. Abe, Y. Matsuo, DNS of turbulent heat transfer in channel flow with respect to Reynolds and Prandtl number effects, *Int. J. Heat Fluid Flow* 20 (1999) 196–207.
- [40] R.A. Antonia, J. Kim, Turbulent Prandtl number in the near wall region of a turbulent channel flow, *Int. J. Heat Mass Transfer* 34 (1991) 1905–1908.
- [41] H. Tennekes, J.L. Lumley, *A First Course in Turbulence*, MIT Press, Cambridge, MA, 1972, pp. 95–97.
- [42] G. Hetsroni, J.L. Zakin, A. Mosyak, Low-speed streaks in drag-reduced turbulent flow, *Phys. Fluids* 9 (1997) 2397–2404.